Fatigue of Materials II Advances and Emergences in Understanding
Edited by: T.S. Srivatsan, M. Ashraf Imam, and R. Srinivasan
TMS (The Minerals, Metals & Materials Society), 2013

THE HIGH CYCLE FATIGUE, DAMAGE INITIATION, DAMAGE PROPAGATION and FINAL FRACTURE BEHAVIOR of ALUMINUM ALLOY 2024

T.S. Srivatsan[1], Satish Vasudevan[2] and K. Manigandan[3]

1: ***Professor***
3: Graduate Student
Department of Mechanical Engineering
The University of Akron
Akron, Ohio 44325-3903, USA
E-Mail: tss1@uakron.edu

2: *Product Development Engineer*
[Custom Engineering]
Navistar, Inc.
2701 Navistar Drive, Lisle, IL 60532
E-Mail: Satish.Vasudevan@Navistar.com

ABSTRACT

In this technical paper the results of a study aimed at understanding the high cycle fatigue properties and fracture characteristics of aluminum alloy 2024 is presented and discussed. Specimens of the alloy in the T-8 temper were cyclically deformed over a range of stress amplitudes at ambient temperature and at a stress ratio of 0.1. Specimens of the alloy were taken from the longitudinal orientation of the as-provided plate and cyclically deformed. The influence of alloy temper (T8 versus T3) on cyclic fatigue life under stress amplitude control is briefly discussed. At the ambient test temperature, the macroscopic fracture mode was essentially identical with specific reference to the magnitude of cyclic stress amplitude. The microscopic mechanisms governing cyclic deformation, fatigue life and final fracture behavior are discussed in light of the mutually interactive influences of magnitude of applied stress, intrinsic microstructural effects, deformation characteristics of the alloy microstructure and macroscopic fracture mode.

Key Words: aluminum alloy, microstructure, cyclic fatigue, stress amplitude, fracture behavior

Introduction

Noticeable strides in both engineering and technology-related applications coupled with an increased emphasis and importance given in the aerospace industry, which successfully pushed technology to its limits, to one that is largely dictated by both commercial interests and concurrent need, did provide the much needed interest, inspiration, inspiration and impetus for developing new, improved and essentially low cost alloys as viable replacements to the material currently being used [1-3]. Both current and emerging technology requirements have placed an increased emphasis on issues like off-the shelf availability, lower weight, damage tolerance, durability, fabric ability, high life-cycle design and even cost effectiveness as primary consideration in governing not only the development of materials but also their selection and use [4-6]. During the past three decades more than one approach has been tried in developing alloys that can provide the desired properties at room temperature in addition to possessing strength at high temperatures and high temperature super-plastic formability. In particular, the alloys of aluminum having during the last four decades, since the early 1970's, engendered a combination of scientific and technological interest for use in a spectrum of high performance applications spanning the industries of aerospace, automotive and even commercial products. The growing need for aluminum alloys that offer a combination of good fracture toughness, high strength, adequate damage tolerance, good high cycle fatigue resistance and even acceptable corrosion resistance that will enable their use in airframe structures and army armaments led to sustained efforts aimed at the development of new and improved alloys, tempers and even their composite counterparts [3,6,7]. It has been safely predicted that most of the aluminum alloys and its advanced or emerging variations currently being produced will find use for those applications that did not exist three or four decades ago [6]. The present markets for aluminum and its alloys are greatly affected by shortages of the other metal counterparts coupled with a combination of economical, environmental and safety factors [7]. In more recent years, the technology related to both aluminum and alloys have grown stronger with competition, i.e., with an increased emphasis on both physical and mechanical properties of the alloys themselves and the dominant role they play in structural applications.

The domain of high cycle fatigue (HCF) corresponds to small applied stress that is essentially confined to the linear region of the stress versus strain curve obtained in a simple tension test. The resultant number of cycles-to-failure (N_f) is high and often greater than 10^4 cycles. It usually comprises of two distinct stages, which have been traditionally referred to as Stage I and Stage II [8]. During Stage I, for polycrystalline metallic materials without defects or inclusions, the cracks, both microscopic and macroscopic in size, appear along the slip bands in grains that are favorably oriented with respect the major stress axis and subsequently tend to follow the preferential slip systems in the adjacent or neighboring grains [8-10]. This stage is generally influenced by intrinsic microstructural features of the alloy. During Stage II the fine microscopic cracks tend to propagate easily along those planes having a maximum normal stress [8,9]. For a polycrystalline ductile solid that is subjected to high cycle fatigue, Stage I is expected to be much larger than Stage II and therefore the number of cycles to failure

(N_f) is strongly dependent on microstructure. The intrinsic microstructural features exert a profound influence on the following: (i) the kinetics of crack initiation, (ii) early microscopic and macroscopic crack growth through the alloy microstructure, (iii) ensuing stable crack growth through the microstructure, and (iv) crack arrest depending on orientation of the grain with respect to the far-field stress axis. This partially explains the scatter that is likely to occur at the fine microscopic level and is quantified by the number of cycles-to-failure [11].

The primary objective of this experimental study was to provide an insight into the high cycle fatigue and final fracture behavior of aluminum alloy 2024 in the T8 temper. The high cycle fatigue response and final fracture behavior are discussed in light of the mutually interactive influences of magnitude of maximum cyclic stress, intrinsic microstructural effects, matrix deformation characteristics and macroscopic aspects of fracture.

Material and Sample Preparation

The material chosen and used in this experimental study was rolled aluminum alloy 2024 plate provided by the Boeing Commercial Airplane Company. The as-provided plates had a thickness of 3-mm. The nominal chemical composition of the Al-Cu-Mg alloy is given in Table 1. Test specimens for the mechanical tests (tension and cyclic fatigue) were precision machined from the as-provided plate stock and conformed to specifications outlined in Standard ASM E-8-10 [Standard Method for Tensile Testing of Metallic Materials] [12] and ASTM E-466-10 [Standard test Method for Stress Amplitude Controlled High Cycle Fatigue Tests on Metallic Materials] [13]. All of the test specimens were precision machined from the as-provided plate stock such that the major stress axis was along the longitudinal direction of the plate. To minimize the extrinsic influence of surface irregularities and finish, and considering surface sensitiveness of the samples prepared from the as-provided material, abundance of care was taken during handling of the test specimens up until testing them on the servo-hydraulic mechanical test machine. To minimize the effects of surface irregularities and finish, final surface preparation of each machined test specimen was achieved by mechanical polishing the gage section using progressively finer grades of silicon carbide impregnated emery paper with the purpose of removing any and all circumferential scratches and surface machining marks.

Experimental Procedures

Initial Microstructure Characterization.

Samples for metallography observation were cut from the as-provided plate stock of alloy 2024-T8. The cut samples, measuring 25 mm square in cross-section, were mounted in bakelite and then wet ground on progressively finer grades of silicon carbide impregnated emery paper using copious amounts of water both as a lubricant and as a coolant. Subsequently, the ground samples were mechanically polished using five-micron and one-micron aluminum oxide (Al_2O_3) powder suspended in distilled water as the lubricant.

The polished aluminum alloy sample was etched using Keller's reagent (a solution mixture of hydrofluoric acid, concentrated nitric acid and distilled water). The etched surface of the sample was observed in an optical microscope and photographed using standard bright field illumination technique.

Mechanical Testing

All mechanical tests were performed up until failure on a fully-automated, closed-loop servo-hydraulic mechanical test machine (INSTRON) equipped with a 100 KN load cell. The specimens were deformed in uniaxial tension at a constant strain rate of 0.0001/sec. The tests were performed in ambient temperature laboratory air environment (Relative Humidity of 55 pct, Temperature = 25°C). Cyclic stress-amplitude controlled high cycle fatigue tests were conducted at ambient temperature (25°C) at a constant cyclic frequency of 5Hz and stress ratio [R = minimum stress/maximum stress = 0.1]. The stress and corresponding number of cycles-to-failure (N_f) were recorded on a PC-based data acquisition system.

The yield strength value obtained from the uniaxial tensile test was used to calculate the maximum stress for the cyclic fatigue tests. At the chosen stress ratio the fatigue tests were conducted over a range of stress amplitudes to establish the variation of maximum stress ($\sigma_{maximum}$) with fatigue life (N_f).

Failure-Damage Analysis

Fracture surfaces of the cyclically deformed and failed specimens were carefully examined in a scanning electron microscope (SEM) over a range of allowable magnifications to:

(a) Determine the macroscopic fracture mode.

(b) Characterize the fine scale topography and features on the fatigue fracture surface for the purpose of establishing (i) the nature of crack initiation, (ii) nature of crack propagation through the alloy microstructure, and (iii) other intrinsic mechanisms governing fracture at the fine microscopic level.

Samples for SEM observation were obtained from the failed fatigue specimens by sectioning parallel to the fatigue surface.

Results and Discussion

Initial Microstructure

The microstructure of the as-provided 2024-T8 alloy plate is shown in **Figure 1**. The microstructure was fully recrystallized with fairly large recrystallized grains that were flattened and elongated along the longitudinal direction as a direct consequence of the mechanical deformation induced by the rolling operation. All of the micrographs were taken immediately below the surface of the specimen chosen. The recrystallized grains were observed to be non-uniform in size and shape. The coarse second-phase particles were found to be randomly distributed through the alloy microstructure with clustering or

agglomeration occurring at regular intervals. A careful examination of the polished sample surface revealed few of the coarse second-phase particles to be decorating the high angle grain boundaries. The smaller and finer second-phase particles, i.e., the Al_2Cu precipitates, could not be easily observed at the allowable magnifications of the optical microscope used in this study (< 1000X).

Tensile Properties

The ambient temperature tensile properties of the as-provided 2024-T8 plate are summarized in **Table 2**. The results reported are the mean value of duplicate tests. At the end of the test, the values of yield strength (σ_{YS}), ultimate tensile strength (σ_{UTS}), fracture strength ($\sigma_{fracture}$) and elongation-to-failure (ϵ_f) were provided as an output of the PC-based data acquisition system. The yield strength of the candidate alloy was determined by identifying the stress at the point on the engineering stress versus engineering strain curve where a straight line drawn parallel to the elastic portion of the curve, at 0.2 pct offset, intersects the curve. The ductility is reported as elongation-to-failure over a gage length of 12.7 mm (0.5 inch). The strain-to-failure was measured using a clip-on extensometer that was attached to the test specimen at the gage section. The test results reveal only marginal difference in both strength and ductility for the two most widely used tempers of this alloy, i.e., T3 and T8. The yield strength of this alloy is 445 MPa, while its ultimate tensile strength in the T8 temper is 476 MPa, suggesting the occurrence of low strain hardening beyond yield. This is clearly seen in the engineering stress versus engineering strain curve shown in **Figure 2**. The elongation measured over 12.5 mm gage length was 8.84 percent.

High Cycle Fatigue Response

The primary purpose of the stress amplitude-controlled fatigue tests is to establish the influence of maximum stress on fatigue life. At low values of the maximum stress the material can be cycled indefinitely, defined in this study as cycles-to-failure in excess of one-million (10^6) cycles. Many metals, to include the ferrous-based family, exhibit a well-defined endurance limit. The endurance fatigue limit is the stress below which the material does not fail. In this experimental study the tests were set to terminate at 10^6 cycles and if failure did not occur in this cycle period the chosen sample is taken to have an infinite life at this stress level. A difference in cyclic fatigue life between the test specimen deformed at a maximum stress near the endurance limit and a higher maximum stress is distinctly evident or noticeable. For most practical applications the material is assumed to have infinite life at and below the endurance limit.

Pure aluminum and its alloys are regarded as not having a plateau in the maximum stress versus fatigue life relationship, unlike the characteristics shown by other non-ferrous metal counterparts having BCC and HCP crystal structures and even the ferrous-based alloys. In this study, an arbitrary cut-off value of 10^6 cycles was used to establish the endurance limit. The results of the axial stress amplitude-controlled fatigue tests is shown in **Figure 3** in which the maximum stress ($\sigma_{maximum}$) is plotted as a function of cycles-to-failure (N_f). The maximum stress ($\sigma_{maximum}$) versus fatigue life (N_f) curve

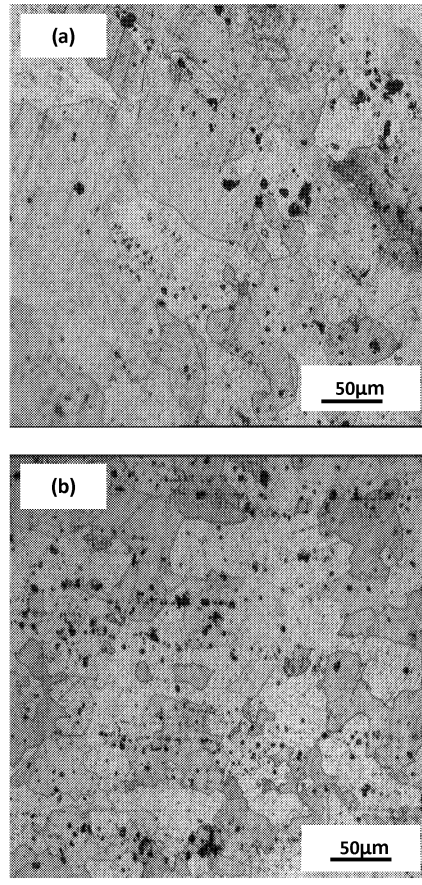

Figure 1. **Optical micrographs showing microstructure of aluminum alloy 2024-T8 (a) Longitudinal direction, and (b) Transverse direction**

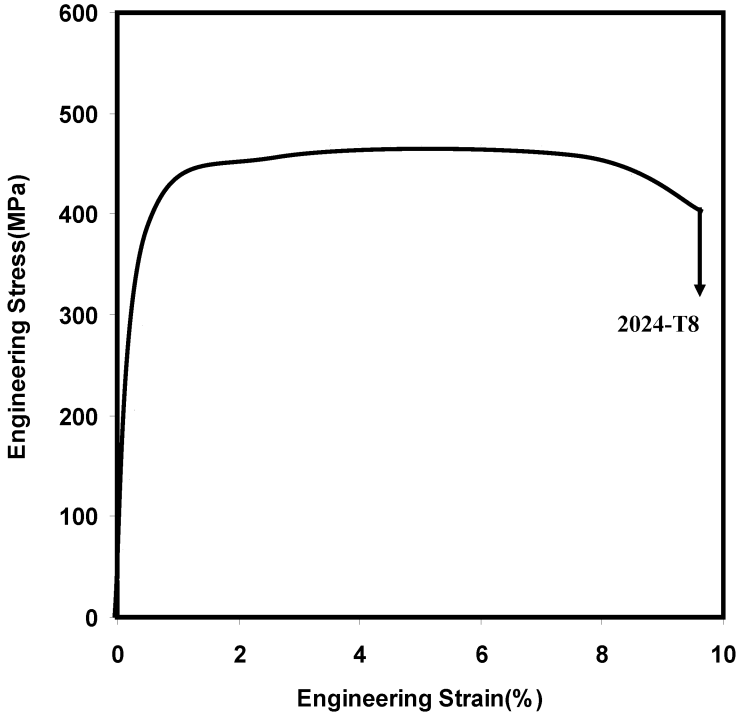

Figure 2. **Variation of engineering stress with engineering strain for aluminum alloy 2024-T8**

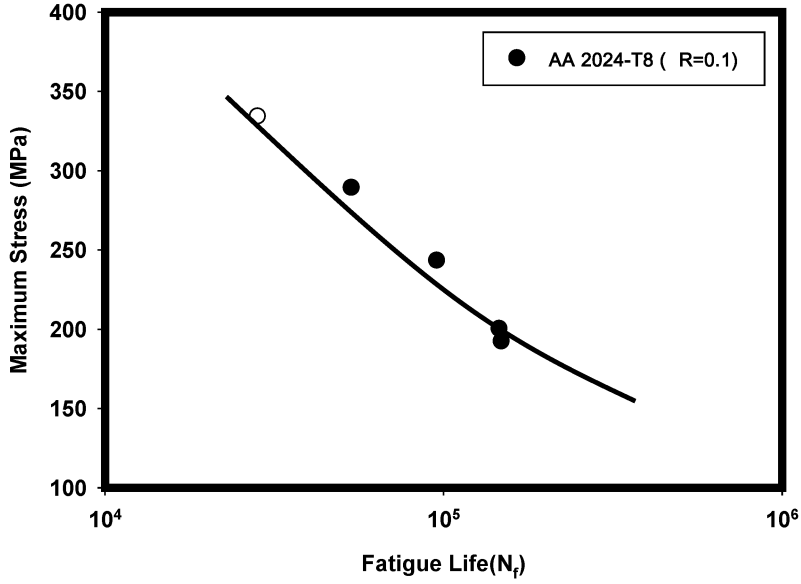

Figure 3. Variation of maximum stress ($\sigma_{maximum}$) with fatigue life (N_f) for aluminum alloy 2024-T8 when deformed at room temperature and at load ratio of 0.1.

reveals a trend of increasing fatigue life with decreasing maximum stress, a behavior shown by (i) other aluminum alloys belonging to the 2XXX series, (ii) most non-ferrous metals, and (iii) their composite counterparts [14-18]. However, the observed trend of increasing fatigue life with decrease in maximum stress is different from those shown by few other face-centered cubic metals that exhibit a well-defined endurance limit [8, 15, 18].

To understand and establish the influence of alloy plate ductility on high cycle fatigue response, quantified by cyclic fatigue life, the maximum stress-fatigue life test data is re-plotted in terms of elastic strain amplitude in a manner suggested and recommended by Hassen and co-workers [19], where the maximum elastic strain ($\sigma_{maximum}$ / E) is the maximum stress normalized by elastic modulus of the specimen in the specific orientation of the alloy plate. Variation of maximum elastic strain with fatigue life is shown in **Figure 4** and reveals a linear trend. This is done to essentially account for the influence of stiffness of the aluminum alloy as a function of test specimen orientation. In an attempt to rationalize the intrinsic influence of microstructure of the alloy plate on high cycle fatigue response, the maximum stress is normalized with respect to ultimate

tensile strength (UTS) and its variation with fatigue life quantified in terms of cycles to failure (N_f) as shown in **Figure 5**

A comparison of the maximum stress versus fatigue life response of this alloy in the T8 temper with alloy 2024 in the T3 temper and alloy 2524 in the T3 temper at a constant load ratio of 0.1 is shown in **Figure 6**. This figure reveals the alloy in the T8 temper to have noticeably inferior fatigue resistance when compared to the same alloy in the T3 temper and the commercial aluminum alloy 2524 at all values of maximum stress. At equivalent values of maximum stress, and identical load ratio of 0.1, the degradation in cyclic fatigue life experienced by the T8 temper is as high as 300 percent over the entire range of stress when compared with the T3 temper.

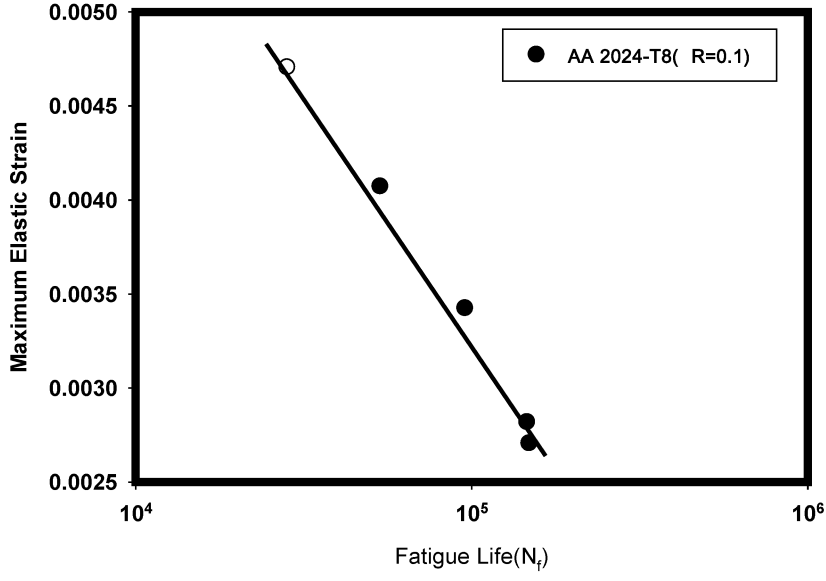

Figure 4. **Variation of maximum elastic strain ($\sigma_{maximum}$ / E) with fatigue life (N_f) for aluminum alloy 2024-T8 cyclically deformed at load ratio of 0.1.**

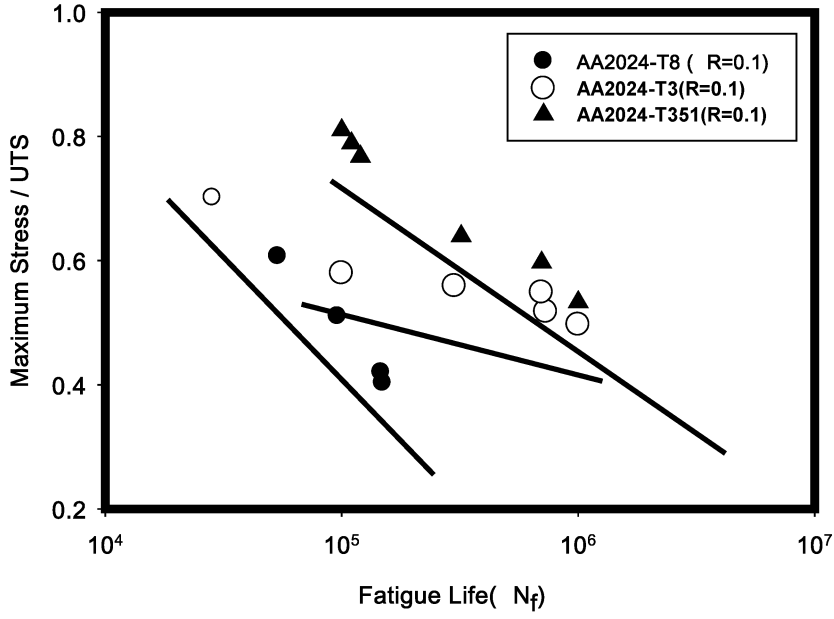

Figure 5. **The variation of ratio of maximum stress / tensile strength [$\sigma_{maximum}/\sigma_{UTS}$] with fatigue life ($N_f$) for aluminum alloy 2024-T8.**

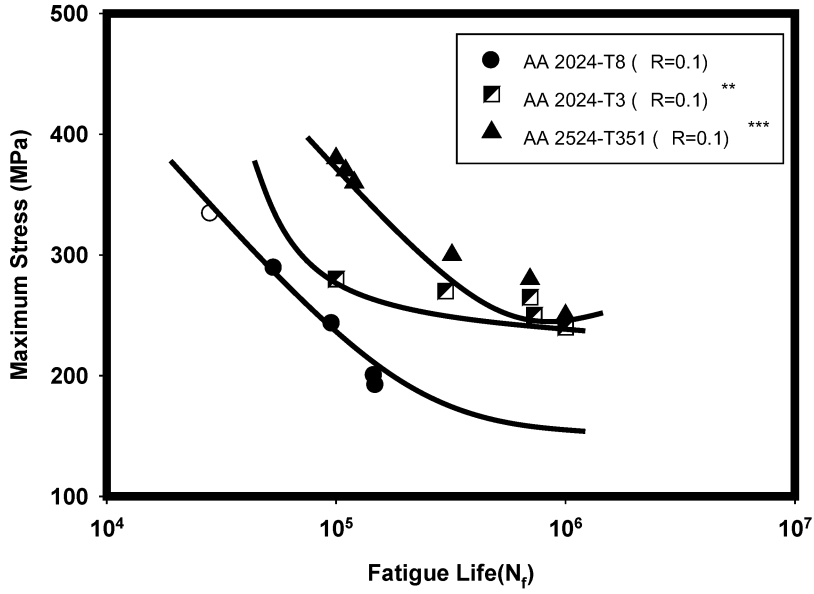

Figure 6. **A comparison of maximum stress versus fatigue life response of aluminum alloy 2024 in the T8 temper with the T3 temper and alloy 2524 in the T351 temper when cyclically deformed at a load ratio of 0.1.**
**** from Reference 15; *** from Reference 19**

High Cycle Fatigue Fracture

Examination of the fracture surfaces of the cyclically deformed and failed test specimens was done in a JEOL scanning electron microscope (SEM) at:

(i) Low magnifications to identify the regions specific to fatigue crack initiation and final fracture (overload).

(ii) At higher allowable magnifications in the fatigue and overload regions to identify the regions of microscopic crack formation, early microscopic growth and other fine scale features on the fracture surface.

Representative fracture features of the deformed and failed test specimens taken from: (i) high maximum stress resultant short fatigue life, and (ii) low maximum stress and resultant enhanced fatigue life, are shown in **Figures 7-9.**

At the load ratio of 0.1 and a maximum stress of 334 MPa the macroscopic fracture mode was essentially normal to the far field stress axis (**Figure 7-a**). High magnification

observation of the cyclic fatigue fracture surface in the region of early microscopic crack growth revealed microscopic voids of varying size and shape along with fine microscopic cracks **(Figure 7-b).** In the region immediately prior to the onset of unstable crack growth and overload the fracture surface revealed a population of dimples and macroscopic voids intermingled with fine microscopic voids. These features are clearly indicative of the occurrence of locally ductile failure mechanisms **[Figure 7-c]**. Well into the region of unstable crack growth the fracture surface revealed the coalescence of the fine microscopic cracks to form a macroscopic crack prior to failure by separation (**Figure 7-d**).

Sample of this 2024-T8 alloy that was cyclically deformed at a lower value of maximum stress, i.e., 243 MPa with a resultant fatigue life of 95,877 cycles, the overall fracture surface morphology was essentially normal to the far-field stress axis **(Figure 8-a**). High magnification observation of the region of stable microscopic crack growth revealed a combination of voids of varying size, dimples, few and far between fine microscopic cracks (**Figure 8-b**). These features are indicative of the ductile and brittle failure mechanisms occurring at the local level. The region of early unstable crack growth revealed cracked second-phase particles intermingled with fine microscopic voids (**Figure 8-c)**. These features are reminiscent of the occurrence of both brittle and ductile failure mechanisms at the fine microscopic level. The region of unstable crack growth was distinct and revealed an observable population of shallow dimples adjacent to the propagating macroscopic cracks (**Figure 8-d).**

Sample of the alloy that was cyclically deformed at a lower maximum stress of 200 MPa and resultant enhanced fatigue life of 146.684 cycles the transgranular fracture regions of the sample surface revealed voids, dimples and intermingled with microscopic cracks (**Figure 9-a**). Careful high magnification observation of the transgranular region revealed the dimples to be of varying size and shape (**Figure 9-b).** Approaching the region of unstable crack growth and immediately prior to failure the fracture surface revealed a combination of microscopic voids and cracked particles (**Figure 9-c**); features indicative of the occurrence of both ductile and brittle failure mechanisms at the local level.

Mechanisms Governing Cyclic Fatigue Fracture

During cyclic deformation of this precipitation hardened aluminum alloy (i.e., 2024) in the T8 condition or temper there does exist a tendency for localized inhomogeneous deformation arising from repeated shearing or destruction of the matrix strengthening precipitates at the fine microscopic level [3, 21-23]. This gradually results in the localization of deformation and resultant accumulation if strain at the fine microscopic level. When the local concentration of stress as a direct consequence of localization of strain at the coarse second phase particles and grain boundaries, exceeds the stress that is required for crack nucleation, microscopic crack initiation is favored to occur [22-24]. The presence of an observable population of both coarse and intermediate size second-phase particles in the alloy microstructure coupled with a microstructure, i.e., the T8 temper, which favors localized inhomogeneous deformation, is conducive for the

nucleation, growth and eventual coalescence of the fine microscopic void to occur at the applied level of maximum cyclic stress.

The initiation of the fine microscopic cracks in the alloy microstructure and their concurrent growth during repeated cyclic loading can be ascribed to the progressive accumulation of micro-plastic deformation at the localized level. The accumulation of micro-plastic damage is exacerbated by stress-microstructure interactions that occur during each cycle of loading. It is this irreversible plastic deformation that is responsible for the initiation and resultant growth of both the fine microscopic cracks and macroscopic cracks through the alloy microstructure. The presence of voids, of varying size and shape, transforms the polycrystalline aluminum alloy to a composite with the voids being safely considered as particles having zero stiffness [24-26]. The initiation of the fine microscopic voids at the coarse second-phase and intermediate size particles in the alloy microstructure and their incremental growth during repeated cyclic deformation culminating in their coalescence does enable in providing small increments of crack tip extension. The finer voids are favored to form at the intermediate-size and smaller size second-phase particles dispersed through the alloy microstructure. Since the voids are intrinsically softer than the hardened grains in the alloy matrix, the local strain is significantly elevated for the microscopic voids causing as a result an increase in their volume fraction during continued cyclic loading.

Table 1: Nominal chemical composition of Aluminum Alloy 2024 (In weight percent)

Cu	Mg	Mn	Fe	Si	Zn	Ti	Aluminum
4.45	1.36	0.71	0.5	0.5	0.2	0.15	Balance

Table 2: Room temperature tensile properties of aluminum alloy 2024

Material	Temper	Elastic Modulus (GPa)	Yield Strength (MPa)	UTS (MPa)	Elongation GL=0.5" (%)
AA 2024	T8	71	445	476	8.84
	T3	73.1	345	483	18
	T4	73.1	324	469	19

Conclusions

Based on a study of the high cycle fatigue and final fracture behavior of aluminum alloy 2024 in the T8 temper, following are the key findings:

1. The as-provided alloy plate revealed large recrystallized grains of non-uniform size and shape with a non-uniform distribution of the coarse second phase particles. At frequent intervals particle agglomeration or clustering was evident.

2. The yield strength of the alloy plate in the T8 temper is noticeably higher than the yield strengths in the T3 and T4 temper. The ultimate tensile strength is about similar in the T8, T3 and T4. In the T8 temper the ultimate tensile strength is only marginally higher than the yield strength indicating low strain hardening capability of the alloy beyond yield.

3. The maximum stress versus fatigue life (N_f) curve reveals a trend that is shown by most non-ferrous metals and their composite counterparts. However, the observed trend is different from those shown by other face-centered cubic metals that exhibit a well-defined endurance limit.

4. At equivalent values of maximum stress the fatigue life of the alloy sample in the T8 temper is noticeably inferior to the T3 temper and the commercially aluminum alloy 2524 in the widely used T3 temper.

5. For this as-provided alloy plate fatigue fracture surface revealed noticeably different topographies at the different values of maximum stress. On a fine microscopic scale the nature, morphology and volume fraction of the intrinsic features on the fatigue fracture surface were found to vary with maximum stress and resultant fatigue life.

6. The presence of a noticeable population of voids of varying size, dimples of varying size and shape and intermingled with microscopic and macroscopic cracking along the grain boundaries is indicative of the occurrence of both ductile and brittle failure mechanisms at the fine microscopic level.

Acknowledgements:

The authors (TSS, SV and MK) extend sincere thanks, gratitude and appreciation to The **BOEING Commercial Aerospace Company** (***Phantom Division***, St Louis, MO, USA) for providing the material used in this study and for funding this research exercise.

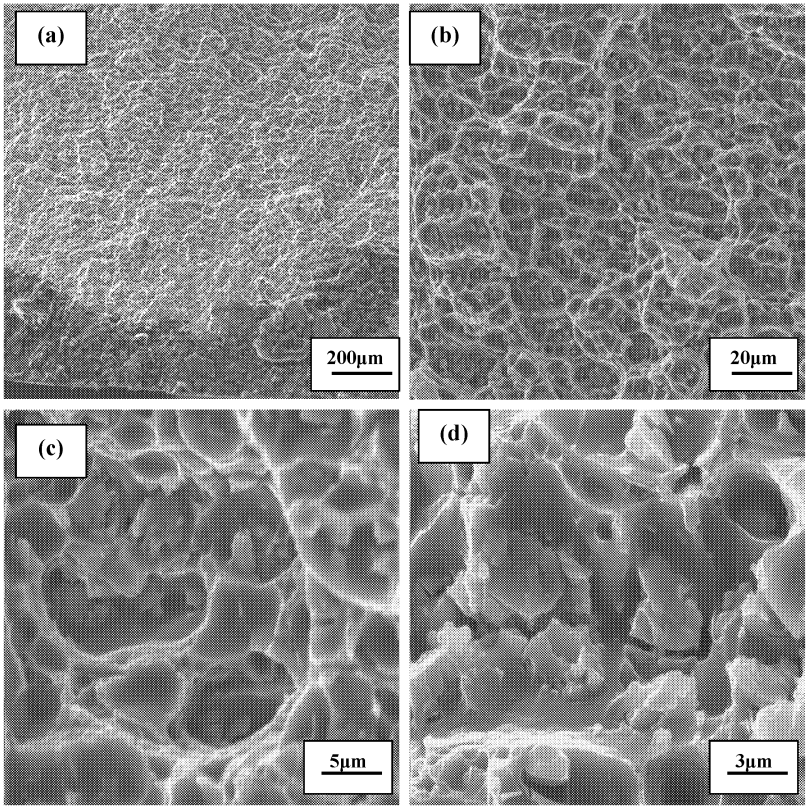

Figure 7. **Scanning electron micrographs of the high cycle fatigue fracture surface of aluminum alloy 2024-T8 deformed at maximum cyclic stress of 334 MPa (R = 0.1), fatigue life = 28,344 cycles, showing**

(a) Overall morphology

(b) High magnification of (a) showing microscopic voids of varying size and shape along with fine microscopic cracks.

(c) Dimples, macroscopic voids and microscopic voids in the region of unstable crack growth

(d) Microscopic cracks coalesce to form a macroscopic crack in the region of unstable crack growth.

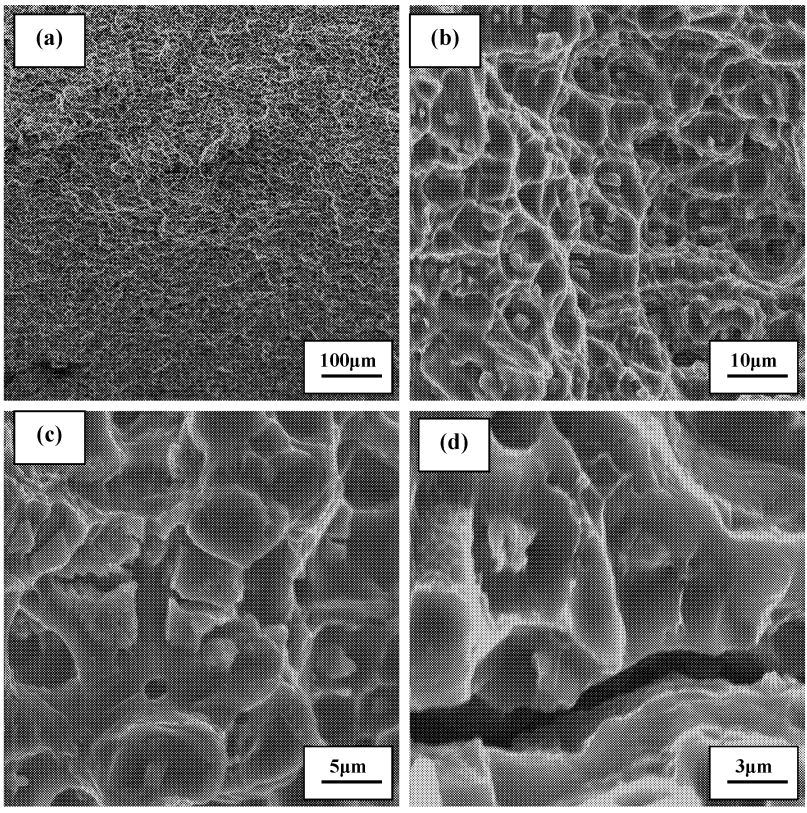

Figure 8. **Scanning electron micrographs of the high cycle fatigue fracture surface of aluminum alloy 2024-T8 deformed at maximum cyclic stress of 243 MPa (R = 0.1), fatigue life = 95,877 cycles, showing**

- **(a) Overall morphology**
- **(b) High magnification of (a) showing voids of varying size, dimples and microscopic cracks.**
- **(c) Cracked particles and microscopic voids in the region of unstable crack growth**
- **(d) Shallow dimples adjacent to macroscopic crack in the region of unstable crack growth.**

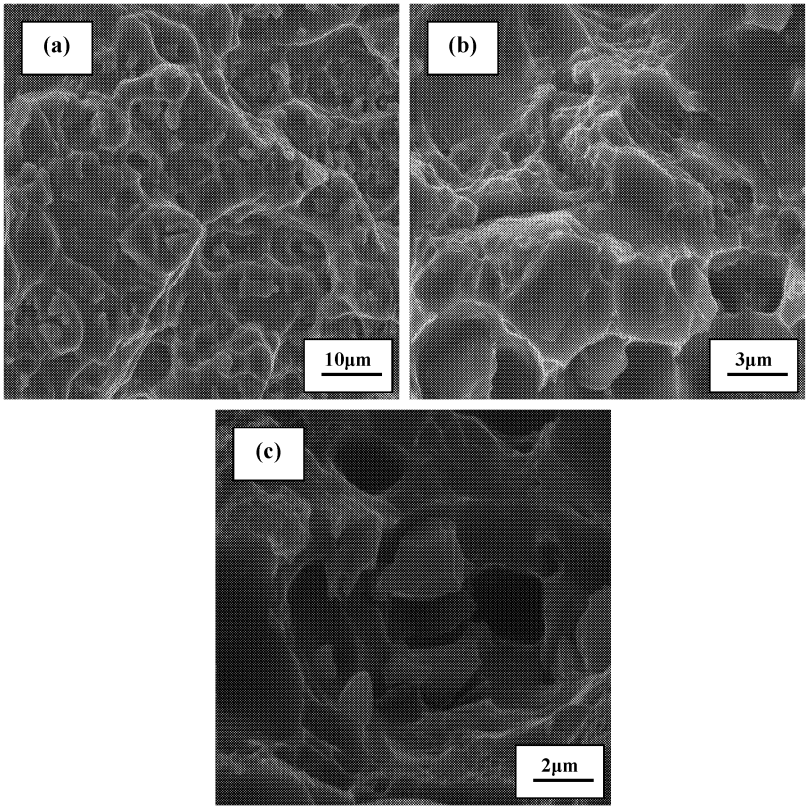

Figure 9. **Scanning electron micrographs of the high cycle fatigue fracture surface of aluminum alloy 2024-T8 deformed at maximum cyclic stress of 200 MPa (R = 0.1), fatigue life = 146,684 cycles, showing**

- **(a) Voids, dimples and microscopic cracks on the transgranular fracture surface**
- **(b) High magnification of (a) showing dimples of varying shape and size.**
- **(c) Microscopic voids and cracked particle in the region of unstable crack growth.**

References

1. E.A. Starke, Jr., in *Aluminum Alloys: Contemporary Research and Applications* (editors: A. K. Vasudevan and R. D. Doherty), Treatise in Materials Science and Technology, Academic Press, Volume 31, 1989, pp. 35-45.
2. A.K. Vasudevan, R.D. Doherty and S. Suresh: in *Aluminum Alloys: Contemporary Research and Applications* (edited by A.K. Vasudevan and R. D. Doherty), Treatise in Materials Science and Technology, Academic Press, Volume 31, 1989, pp. 446-456.
3. J.T. Staley: Aluminum Alloys and Composites, in *Encyclopedia of Physical Science,* Vol. 1, 1992, pp. 591-611.
4. R. Grimes, M. J. Stowell and B. M. Watts: **Metals Technology**, Vol. 3, 1976, pp. 154-155.
5. R.H. Bricknell and J.W. Edington: **Metallurgical Transactions**, Vol. 10Am, 1979, pp. 1257-1267.
6. Aluminum Alloys in the 1970s: **Metal Progress**, September 1970, pp. 68-79.
7. M. O. Speidel: **Metallurgical Transactions**, Vol. 6A, 19875, pp. 631-640.
8. S. Suresh: *Fatigue of Materials*, Cambridge University Press, Cambridge United Kingdom, 1991.
9. H.J. Miller: **Fatigue of Engineering Materials and Structures**, Vol. 5, 1982, pp. 223-232.
10. J. Lankford: **Fatigue of Engineering Materials and Structures**, Vol. 5, 1982, pp. 233-243.
11. M. Sauzay and T. Jourdan**: International Journal of Fracture**, Vol. 141, 2006, pp. 431-466.
12. American Society for Testing and Materials: Standard E-8-10: "*Conducting Tension Test on Metallic Materials*," American Society for Testing and Materials (ASTM), Philadelphia, PA, USA, (2010).
13. American Society for Testing and Materials: Standard E-466-02: "*Conducting Constant Amplitude Axial Fatigue Tests on Metallic Materials*," American Society for Testing and Materials (ASTM), Philadelphia, PA, USA, (2002).
14. T. S. Srivatsan and M. Al-Hajri: **Composites**, Part B, Viol. 33, 20023, pp. 391-404.
15. T.S. Srivatsan, S. Vasudevan, Lisa Park and R. J. Lederich: **Materials & Design**, 2007,
16.
17. U. Alfaro, T. Ghidini and C. Dalle Donne**: "**Fatigue of pre-corroded 2024-T3 Friction Stir Welds' Experiment and Prediction",.
18. Fatigue and Fracture Handbook, ASM Metals Handbook Volume 19, American Society for Materials International, Materials Park, Ohio, 2009, pp.
19. D.F. Hassen, C.R. Crowe, J.S. Ahearn and D.C. Cooke: *Failure Mechanisms in High Performance Materials* (edited by J.E. Early, T.R. Shives and J.H. Smith), The Minerals, Metals and Materials Society, TMS, Warrendale, PA, USA, 1984, pp. 147-157

20. T.S. Srivatsan, Nurudeen Balogan and T. Quick in *Fatigue of Materials: Advances and Emergences in Understanding* (edited: T.S. Srivatsan and M. Ashraf Imam) The Minerals, Metals and Materials Society, TMS, Warrendale, PA, SA, 2010, pp. 339-354
21. T.S. Srivatsan, S. Anand and P. Magnusen: ***Materials Science and Engineering***, Vol. A314, 2001, pp. 118-123.
22. T.S. Srivatsan, D. Lanning and K. K. Soni: **Journal of Materials Science**, Vol. 28, 1993, pp. 3205-3211.
23. T.S. Srivatsan, S. Sriram, D. Veeraraghavan and V. K. Vasudevan: **Journal of Materials Science**, Vol. 32, 1977, pp. 2883-2889.
24. T.S. Srivatsan and Satish Vasudevan " The Science, Technology and Applications of Aluminum and Aluminum Alloys," *Advanced Structural Materials* (editors: Winston O Soboyejo and T.S. Srivatsan), CRC Press, Taylor & Francis Group, pp. 225-274.
25. R.H. Van Stone and J.A. Psioda: **Metallurgical Transactions**, Vol. 6A, 1975, pp. 672-677.
26. R.H. Van Stone, T.B. Cox, J.R. Low and J.A. Psioda: **International Materials Reviews,** Vol. 30, 1985, pp. 1567-177.